Tolerance Analysis of Near-Field Focused Arrays to Safe-for-Humans Microwave and RF Applications

Giovanni Buonanno, *Member, IEEE*, and Sandra Costanzo, *Senior Member, IEEE*

***Abstract*— A methodology is proposed in this work to characterize the complex vector near-field of focused antenna arrays with arbitrary geometry, subject to random errors. Starting with the problem formulation, a proper mathematical relationship for the actual electric field is established, and a partial statistical characterization is then performed. Subsequently, the mean squared errors are computed between the actual and the desired electric field, and between the actual and the ideal squared magnitude of the electric field. Finally, a method to determine the cumulative distribution function (cdf) of the squared magnitude of the electric field is discussed for obtaining appropriate percentile functions. The presented numerical results show the validity of the proposed technique, which is particularly useful in those applications, such as the biomedical ones, where high performance is required to control the electric field values such to guarantee human safety conditions.**

***Index Terms*— Antenna arrays, antenna focusing, biomedical applications, health safety, near-field, tolerance analysis.**

I. Introduction

THE theory of near-field focused antenna arrays (NFFAs) is attracting increasing interest since many years [1], [2], [3], [4], due to their consolidated high potential for a number of applications, such as identification systems, industrial microwave applications, microwave power transmissions, antenna measurements, and biomedical applications [5], [6], [7], [8]. NFFAs are able to concentrate/receive the field at/from points located in the near-zone of the array [9]. Therefore, for such systems, the principle of pattern multiplication, very advantageously employed in far-field focused arrays, cannot be exploited, as it is not possible to identify the array factor and to isolate a vector field acting as a radiation pattern common to all the antenna elements. Consequently, the study of NFFAs is more challenging as compared to antenna arrays for far-field applications. The above difficulty can be also recognized in the context of focused aperture antennas [10].

Near-field focused arrays, as well as arrays designed for far-field applications, suffer from various imperfections that lead to *distortions* of the (desired) field. In fact, even if meticulously designed, antenna arrays have to face both random uncorrelated and spatially correlated errors that can be due to manufacturing tolerances, element failures, aging, finite representation of the magnitudes and phases of the excitation coefficients, frequency variations, mutual coupling, perturbations of the control signals in the feeding network [9], [10], [11], [12]. Usually, spatially correlated errors can be minimized and, therefore, random uncorrelated errors are preeminent [12]. As a result, it is advantageous to consider and properly address the presence of such errors in the design stage.

To the best of the authors' knowledge, the analysis and/or synthesis of antenna arrays in the presence of random errors (tolerance theory [11]) has been mainly focused on far-field applications. The first pioneering works in this sense date back to the 1950s and 60s, due to Ruze [13], [14], Ashmead [15], Gilbert and Morgan [16], Rondinelli [17], Elliott [18], and Allen [19]. Interesting results have been presented also by Hsiao [20], [21] and Kaplan [22]. These authors have studied the effect of random errors, mainly in relation to:

1) The behavior of the mean of the squared magnitude of the array factor.
2) The distribution of the squared magnitude of the array factor.
3) The antenna array gain.

Also, some results have been provided in relation to the distribution of the peak sidelobe level. The interested reader can find in-depth discussions of the tolerance theory of far-field antenna arrays in [11], [12], [23], and [24]. Interesting results have also been obtained in statistical antenna theory [25]. It is worth highlighting that the problem of random errors in antenna arrays is still a current problem that needs to be adequately taken into account [26], [27], [28]. It is also worth noting that tolerance theory shares strong similarities with the probabilistic analysis/synthesis of nonuniformly spaced (far-field) antenna arrays [29], [30], [31], [32], [33], [34], [35]

Manuscript received 6 October 2023; revised 22 March 2024; accepted 26 March 2024. Date of publication 4 April 2024; date of current version 7 May 2024. This work was supported in part by the Ministero dell'Università e della Ricerca (MUR), Italy, as part of "Programma Operativo Nazionale Ricerca e Innovazione 2014–2020" (PON "Ricerca e Innovazione" 2014–2020) Project "Noninvasive Electromagnetic Green Devices and Methods for Advanced Medical Diagnostics"; Project PNRR PE8—Conseguenze e sfide dell'invecchiamento "Age-IT (Ageing well in an ageing society)"; and Piano Operativo Salute (POS) 2021 Project titled "Radioamica—Open Network per la RADIOmica/rAdiogenoMIca Cooperativa basata su intelligenza artificiale"—Traiettoria 2 "E-Health, diagnostica avanzata, medical devices e mini invasività," Azione 2.1 "Creazione di una rete nazionale per le malattie ad alto impatto" del Piano Sviluppo e Coesione Salute—FSC 2014–2020; and as part of Italian National Project PON ARS01_00536 "OCEANOS." *(Corresponding author: Sandra Costanzo.)*

Giovanni Buonanno is with the University of Calabria, 87036 Rende, Italy.

Sandra Costanzo is with the University of Calabria, 87036 Rende, Italy, also with Inter-University National Research Center on Interactions Between Electromagnetic Fields and Biosystems (ICEmB), 16145 Genoa, Italy, and also with the Consorzio Nazionale Interuniversitario per le Telecomunicazioni, 43124 Parma, Italy (e-mail: costanzo@dimes.unical.it).

Color versions of one or more figures in this article are available at https://doi.org/10.1109/TAP.2024.3383274.

Digital Object Identifier 10.1109/TAP.2024.3383274

and the collaborative beamforming in ad hoc sensor networks [36].

A probabilistic study of random uncorrelated errors in Fresnel-zone focused antenna arrays has recently been presented in [37]. Such work has adapted tolerance theory methodologies for far-field focused arrays to the radiative near-field region, providing a general approach together with some approximations based on recently introduced results [38] for estimating the cumulative distribution function (cdf) of a particular function, which acts, in a sense, as a kind of array factor. A general model for NFFAs, subject to random errors, has been recently proposed by Costanzo and Buonanno [39]. Starting from the original development in [39], the present work aims to generalize the methodology in [37], making no assumptions about the geometry of NFFAs to be characterized. Furthermore, the field observation is not restricted to any specific plane, thus fully considering the vector electric field. By modeling the random errors as in [37], the first- and second-order partial statistical functions of the electric field are first provided. Subsequently, the approach presented in [39] is strongly extended through the following enhancements.

1) A simple relation for the variance of the squared magnitude of the electric field is introduced.
2) The statistical characterization is performed for the relation existing between the real and the imaginary parts of the three scalar components of the electric field, through the respective covariance functions that form the covariance matrix.
3) An in-depth discussion is performed regarding some important properties of the above covariance matrix.
4) The modeling of the joint probability density function of the real and imaginary parts of the three scalar components of the electric field is performed by exploiting the multivariate Lindeberg–Feller central limit theorem [40].
5) A method is proposed for determining the cdf of the squared magnitude of the electric field, to introduce appropriate confidence curves.

To develop this model, appropriate covariance functions are considered as a first step. Regardless of whether the covariance matrix related to the aforementioned multidimensional pdf is singular, it is shown that the distribution of the squared magnitude of the electric field can be computed efficiently, by exploiting the spectral decomposition of real and symmetric matrices.

There are several reasons for this work. By now, various applications require very high operating frequencies and systems of large dimensions in terms of wavelength. Consequently, the near-field region undergoes an extension that must be addressed in the design stage [25]. In addition, some applications naturally employ antenna arrays working in the near-field, such as, for example, some biomedical applications [7]. Furthermore, it must be considered that the behavior of the electromagnetic field in the radiative near-field region of antennas is also crucial for problems related to safety at radiation exposure [41]. As a result, it is of paramount importance that the levels of the field are adequately controlled. However, as previously stated, errors affecting the array could harm generating the desired field. Consequently, a methodology that helps take these errors into account and, therefore, be able to predict their effects may be essential.

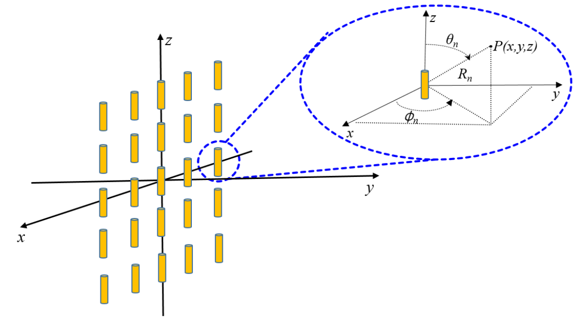

Fig. 1. Representation of a generic array together with the observation variables.

II. Problem Formulation

Let us consider a generic array composed by N radiators which is immersed into a lossless free space-like medium (as an example, in Fig. 1 a periodic planar array is reported). The electric field at the generic point $P \equiv (x, y, z)$ belonging to the near-field region of the array, but located in the far-zone of each radiator, can be written as [42]

$$\mathbf{E}_{id}(P) = K \sum_{n=1}^{N} I_n \frac{e^{-jkR_n}}{R_n} \mathbf{h}_n(P) \tag{1}$$

where $K = (jk\eta)/(4\pi)$, k is the wavenumber in the propagation medium, η is the medium impedance, $I_n = A_n e^{j\alpha_n}$ is the complex feeding current ($A_n \in [0, +\infty]$, $\alpha_n \in [0, 2\pi]$), $R_n = \sqrt{(x-x_n)^2 + (y-y_n)^2 + (z-z_n)^2}$ is the distance between the phase center of the nth element and the point P, (x_n, y_n, z_n) is the position of the phase center of the nth element, and $\mathbf{h}_n(P)$ is the effective length of the nth element evaluated at point P. It is worth highlighting that, even if in Fig. 1 the radiators are assumed to be equally oriented in space, this condition is not mandatory for the purposes of the discussed methodology. In fact, the spherical coordinates R_n, θ_n, and ϕ_n are defined with respect to the reference system of the specific radiator. Furthermore, arrays of any geometry can be analyzed. Moreover, the (ideal) phases of the excitation coefficients are determined by exploiting the conjugate-phase method [7]

$$\alpha_n = kR_{n_f} = k\sqrt{\left(x_f - x_n\right)^2 + \left(y_f - y_n\right)^2 + \left(z_f - z_n\right)^2} \tag{2}$$

where (x_f, y_f, z_f) is the position of the so-called *focal point*. Of course, the present methodology is also valid for near-field multifocused arrays. The conjugate phase method is probably the most used approach, as it is also the simplest one, to realize the focusing condition. However, it does not allow to consider the mutual couplings between the antenna elements [43].

In light of the above, to somehow take into account the effect of mutual couplings between antenna elements [11], while also considering the effects of possible fluctuations in the feeding network, component tolerances, antenna elements faults, and other possible causes of error, it is assumed that as follows [37].

1) The magnitudes and the phases of the excitation coefficients are subject to random additive errors.
2) The actual magnitudes of the excitation coefficients are multiplied by suitable coefficients.

Consequently, the actual electric field can be modeled as follows:

$$\begin{aligned}\mathbf{E}(P) &= K\sum_{n=1}^{N} F_n(A_n+\delta A_n)\,e^{j(\alpha_n+\delta\alpha_n)}\frac{e^{-jkR_n}}{R_n}\,\mathbf{h}_n(P)\\ &= K\sum_{n=1}^{N} C_n\,h_{n_x}(P)\hat{\mathbf{x}}+\sum_{n=1}^{N} C_n\,h_{n_y}(P)\hat{\mathbf{y}}+\sum_{n=1}^{N} C_n\,h_{n_z}(P)\hat{\mathbf{z}}\\ &= E_x(P)\hat{\mathbf{x}}+E_y(P)\hat{\mathbf{y}}+E_z(P)\hat{\mathbf{z}}\end{aligned} \tag{3}$$

with the function C_n given by

$$C_n = F_n(A_n+\delta A_n)\,e^{j(\alpha_n+\delta\alpha_n)}\frac{e^{-jkR_n}}{R_n} \tag{4}$$

and where $F_n \in \{0,1\}$ is a binary random variable that indicates whether the nth element is faulty or turned on, such that $\mathscr{P}_r\{F_n=1\} = 1-\mathscr{P}_r\{F_n=0\} = \overline{F_n} = m_n$, while δA_n and $\delta\alpha_n$ are zero-mean continuous random variables. More precisely, $\{\delta\alpha_n\}_{n=1}^{N}$ are zero-mean Gaussian random variables, while for amplitude errors, there is generally no particular assumption [11], [12]. Moreover, all random variables are independent of each other. It is worth highlighting that the considered errors are the most common ones encountered in antenna arrays [12]. As a further important aspect, the mutual couplings effects are assumed to be sufficiently weak so that no influence is reflected on the shape of the current densities. They are simply modeled by including them into amplitude and phase errors related to the excitation coefficients [11]. From a practical point of view, arrays with sufficiently spaced radiators are considered, so to avoid strong mutual couplings. Anyway, another alternative approach could be to exploit the active-element pattern method including the mutual couplings as incorporated within the active element patterns [12]. In this case, the function $\mathbf{h}_n(P)$ would be linked to the active element pattern of the nth radiator.

As for the active element pattern method, some clarifications may be useful. In particular, for small to medium sized arrays, the characterization of active element patterns can be very demanding from a computational point of view. Instead, such a technique can be advantageous for large arrays, as in this case, it is possible to use the central element pattern method, in which the active element pattern of one of the most central elements of the array is representative of all the other elements [9]. In the case of small to medium sized arrays, it may be more useful to exploit appropriate mutual coupling compensation schemes [44], [45]. For the sake of completeness, it is worth mentioning that technological solutions have also been introduced for the minimization of mutual couplings, such as the adoption of EBG structures [9], [46].

In summary, as previously stated, this article is based on the same philosophy exposed in [11], which states that regardless of which phenomena (including mutual couplings) are responsible for errors, their effect is to modify the magnitudes and phases of the excitation coefficients. This point of view is compatible with the modeling of mutual couplings by means of the isolated-element pattern approach [44], in which all mutual coupling effects are included in the excitation coefficients. Anyway, further studies are currently devoted by the authors to investigate error characterization methods in which mutual couplings can be explicitly included. The results coming from the above studies will be presented in a future work.

Since the functions $\{C_n\}_{n=1}^{N}$ are stochastic processes, it follows that $\mathbf{E}(P)$ is a *random vector field*, which must be studied by exploiting the theory of probability. Moreover, the three complex components of the electric field are mutually dependent. The mean and the variance of the actual electric field can be written as follows (the upper bar denotes the operation of statistical mean):

$$\begin{aligned}\boldsymbol{\mu}(P) &= \overline{\mathbf{E}(P)} = K\sum_{n=1}^{N}\overline{C_n}\,\mathbf{h}_n(P)\\ &= \overline{E_x(P)}\,\hat{\mathbf{x}}+\overline{E_y(P)}\,\hat{\mathbf{y}}+\overline{E_z(P)}\,\hat{\mathbf{z}}\\ &= \mu_x(P)\,\hat{\mathbf{x}}+\mu_y(P)\,\hat{\mathbf{y}}+\mu_z(P)\,\hat{\mathbf{z}}\end{aligned} \tag{5}$$

$$\begin{aligned}\sigma^2(P) &= \overline{|\mathbf{E}(P)-\boldsymbol{\mu}(P)|^2}\\ &= \overline{|E_x(P)-\mu_x(P)|^2}+\overline{\left|E_y(P)-\mu_y(P)\right|^2}\\ &\quad+\overline{|E_z(P)-\mu_z(P)|^2}\\ &= \sigma_x^2(P)+\sigma_y^2(P)+\sigma_z^2(P)\end{aligned} \tag{6}$$

where $\mu_\nu(P)$ and $\sigma_\nu^2(P)$ are the mean and the variance of the scalar component $E_\nu(P)$ (for $\nu = x, y, z$) of the electric field, respectively. The mean $\mu_\nu(P)$ and the variance $\sigma_\nu^2(P)$ can be expressed as follows (for $\nu = x, y, z$):

$$\mu_\nu(P) = K\sum_{n=1}^{N} m_n\,A_n\,e^{j\alpha_n}\,e^{-\frac{\sigma_{\delta\alpha_n}^2}{2}}\,\frac{e^{-jkR_n}}{R_n}\,h_{n_\nu}(P) \tag{7}$$

$$\begin{aligned}\sigma_\nu^2(P) &= \overline{|E_\nu(P)-\mu_\nu(P)|^2} = \overline{|E_\nu(P)|^2}-|\mu_\nu(P)|^2\\ &= |K|^2\sum_{n=1}^{N}\frac{m_n\left(A_n^2-m_n\,A_n^2\,e^{-\sigma_{\delta\alpha_n}^2}+\sigma_{\delta A_n}^2\right)}{R_n^2}\left|h_{n_\nu}(P)\right|^2\end{aligned} \tag{8}$$

and, as it can be seen, the amplitude errors, $\{\delta A_n\}_{n=1}^{N}$, do not affect the mean of the electric field, while the other two types of errors cause the field levels to decrease. As regarding the variance of the electric field, it is affected by all three types of errors and, obviously, in the absence of these, it is equal to zero, just as the mean of the electric field coincides with the ideal electric field.

III. Partial Characterization of the Squared Magnitude of the Electric Field

In several applications, it is essential to properly control the squared magnitude of the electric field, as it is related to the power density. In the present work, the squared magnitude of the electric field is a random function, and therefore it needs to be adequately (probabilistically) characterized. In this section, a partial characterization of $|\mathbf{E}(P)|^2$ is performed, while, in the following, a more specific characterization is discussed, by exploiting a particular assumption between all the real and the imaginary parts of the components of the electric field. The mean of the squared magnitude of the electric field is related to the mean and the variance of the electric field as reported below

$$\begin{aligned}\mu_{|\mathbf{E}|^2}(P) &= \overline{|\mathbf{E}(P)|^2} = |\boldsymbol{\mu}(P)|^2 + \sigma^2(P)\\ &= |K|^2 \sum_{n=1}^{N} \frac{m_n\left(A_n^2+\sigma_{\delta A_n}^2\right)}{R_n^2}\,|\mathbf{h}_n(P)|^2\\ &\quad + |K|^2 \sum_{n=1}^{N}\sum_{q=1,q\neq n}^{N}\left\{m_n\, m_q\, A_n\, A_q\, e^{j(\alpha_n-\alpha_q)}\, e^{-\frac{\sigma_{\delta\alpha_n}^2+\sigma_{\delta\alpha_q}^2}{2}}\right.\\ &\qquad\left.\times \frac{e^{-jk(R_n-R_q)}}{R_n\, R_q}\,\mathbf{h}_n(P)\cdot\mathbf{h}_q^*(P)\right\}\\ &= |\mathbf{E}_{id}(P)|^2 + |K|^2 \sum_{n=1}^{N}\frac{\left(m_n\, A_n^2 + m_n\,\sigma_{\delta A_n}^2 - A_n^2\right)}{R_n^2}\,|\mathbf{h}_n(P)|^2\\ &\quad + |K|^2 \sum_{n=1}^{N}\sum_{q=1,q\neq n}^{N}\left\{\frac{m_n m_q A_n A_q e^{-\frac{\sigma_{\delta\alpha_n}^2+\sigma_{\delta\alpha_n}^2}{2}} - A_n A_q}{R_n R_q}\, e^{j(\alpha_n-\alpha_q)}\right.\\ &\qquad\left.\times e^{-jk(R_n-R_q)}\,\mathbf{h}_n(P)\cdot\mathbf{h}_q^*(P)\right\}\end{aligned}\tag{9}$$

where the symbol * denotes the complex conjugate operation. As it can be easily verified, in the absence of errors, $\mu_{|\mathbf{E}|^2}(P) = |\mathbf{E}_{id}(P)|^2$. It is worth noting that the squared magnitude of the electric field represents a quadratic form. In fact, considering the *multivariate random (algebraic) column vector* $\underline{X}(P) = [E_{x_\Re}(P), E_{x_\Im}(P), E_{y_\Re}(P), E_{y_\Im}(P), E_{z_\Re}(P), E_{z_\Im}(P)]^T$, with $E_{\nu_\Re}(P)$ (resp. $E_{\nu_\Im}(P)$) being the real (resp. imaginary) part of $E_\nu(P)$ (for $\nu = x, y, z$), it can be written that [47]

$$\mu_{|\mathbf{E}|^2}(P) = tr\left\{\underline{\underline{\mathscr{K}}}(P)\right\} + \underline{\mu}^T(P)\cdot\underline{\mu}(P) \tag{10}$$

where

$$\underline{\mu}(P) = \left[\mu_{x_\Re}(P), \mu_{x_\Im}(P), \mu_{y_\Re}(P), \mu_{y_\Im}(P), \mu_{z_\Re}(P), \mu_{z_\Im}(P)\right]^T \tag{11}$$

and (with P implied)

$$\underline{\underline{\mathscr{K}}}(P) = \begin{bmatrix} \sigma_{x_\Re}^2 & \mathscr{K}_{x_\Re x_\Im} & \mathscr{K}_{x_\Re y_\Re} & \mathscr{K}_{x_\Re y_\Im} & \mathscr{K}_{x_\Re z_\Re} & \mathscr{K}_{x_\Re z_\Im}\\ \mathscr{K}_{x_\Re x_\Im} & \sigma_{x_\Im}^2 & \mathscr{K}_{x_\Im y_\Re} & \mathscr{K}_{x_\Im y_\Im} & \mathscr{K}_{x_\Im z_\Re} & \mathscr{K}_{x_\Im z_\Im}\\ \mathscr{K}_{x_\Re y_\Re} & \mathscr{K}_{x_\Im y_\Re} & \sigma_{y_\Re}^2 & \mathscr{K}_{y_\Re y_\Im} & \mathscr{K}_{y_\Re z_\Re} & \mathscr{K}_{y_\Re z_\Im}\\ \mathscr{K}_{x_\Re y_\Im} & \mathscr{K}_{x_\Im y_\Im} & \mathscr{K}_{y_\Re y_\Im} & \sigma_{y_\Im}^2 & \mathscr{K}_{y_\Im z_\Re} & \mathscr{K}_{y_\Im z_\Im}\\ \mathscr{K}_{x_\Re z_\Re} & \mathscr{K}_{x_\Im z_\Re} & \mathscr{K}_{y_\Re z_\Re} & \mathscr{K}_{y_\Im z_\Re} & \sigma_{z_\Re}^2 & \mathscr{K}_{z_\Re z_\Im}\\ \mathscr{K}_{x_\Re z_\Im} & \mathscr{K}_{x_\Im z_\Im} & \mathscr{K}_{y_\Re z_\Im} & \mathscr{K}_{y_\Im z_\Im} & \mathscr{K}_{z_\Re z_\Im} & \sigma_{z_\Im}^2 \end{bmatrix} \tag{12}$$

with $\mu_{\nu_\Re}(P)$ (resp. $\mu_{\nu_\Im}(P)$) and $\sigma_{\nu_\Re}^2(P)$ (resp. $\sigma_{\nu_\Im}^2(P)$) being the mean and variance of $E_{\nu_\Re}(P)$ (resp. $E_{\nu_\Im}(P)$) (for $\nu = x, y, z$), $\underline{\underline{\mathscr{K}}}(P)$ being the covariance matrix associated with the random vector $\underline{X}(P)$, and $tr\{\underline{\underline{K}}(P)\}$ being the trace of $\underline{\underline{\mathscr{K}}}(P)$.

The following covariance function $\mathscr{K}_{\nu_\Re\xi_\Re}(P)$ (for $\nu = x, y, z$ and $\xi = x, y, z$):

$$\begin{aligned}\mathscr{K}_{\nu_\Re\xi_\Re}(P) &= \overline{E_{\nu_\Re}E_{\xi_\Re}} - \overline{E_{\nu_\Re}}\,\overline{E_{\xi_\Re}}\\ &= |K|^2\sum_{n=1}^{N}\left\{\frac{p_n\left(A_n^2+\sigma_{\delta A_n}^2\right)}{R_n^2}\left|h_{n_\nu}\right|\left|h_{n_\xi}\right|\right.\\ &\quad\times\left[\frac{1}{2}\cos\left(\angle h_{n_\xi}-\angle h_{n_\nu}\right)\right.\\ &\quad\left.\left.+\frac{1}{2}e^{-2\sigma_{\delta\alpha_n}^2}\cos\left(2kR_n-2\alpha_n-2\angle K - \angle h_{n_\nu}-\angle h_{n_\xi}\right)\right]\right\}\\ &\quad - |K|^2\sum_{n=1}^{N}\left\{\frac{p_n^2A_n^2}{R_n^2}\left|h_{n_\nu}\right|\left|h_{n_\xi}\right|e^{-\sigma_{\delta\alpha_n}^2}\right.\\ &\quad\times\cos\left(kR_n-\alpha_n-\angle K-\angle h_{n_\nu}\right)\\ &\quad\left.\times\cos\left(kR_n-\alpha_n-\angle K-\angle h_{n_\xi}\right)\right\}\end{aligned}\tag{13}$$

allows to compute $\sigma_{x_\Re}^2(P)$, $\sigma_{y_\Re}^2(P)$, $\sigma_{z_\Re}^2(P)$, $\mathscr{K}_{x_\Re y_\Re}(P)$, $\mathscr{K}_{x_\Re z_\Re}(P)$, and $\mathscr{K}_{y_\Re z_\Re}(P)$. Instead, the following covariance function $\mathscr{K}_{\nu_\Re\xi_\Im}(P)$ (for $\nu = x, y, z$ and $\xi = x, y, z$):

$$\begin{aligned}\mathscr{K}_{\nu_\Re\xi_\Im}(P) &= \overline{E_{\nu_\Re}E_{\xi_\Im}} - \overline{E_{\nu_\Re}}\,\overline{E_{\xi_\Im}}\\ &= -|K|^2\sum_{n=1}^{N}\left\{\frac{p_n\left(A_n^2+\sigma_{\delta A_n}^2\right)}{R_n^2}\left|h_{n_\nu}\right|\left|h_{n_\xi}\right|\right.\\ &\quad\times\left[\frac{1}{2}\sin\left(\angle h_{n_\nu}-\angle h_{n_\xi}\right)\right.\\ &\quad\left.\left.+\frac{1}{2}e^{-2\sigma_{\delta\alpha_n}^2}\sin\left(2kR_n-2\alpha_n-2\angle K - \angle h_{n_\nu}-\angle h_{n_\xi}\right)\right]\right\}\\ &\quad + |K|^2\sum_{n=1}^{N}\left\{\frac{p_n^2A_n^2}{R_n^2}\left|h_{n_\nu}\right|\left|h_{n_\xi}\right|e^{-\sigma_{\delta\alpha_n}^2}\right.\\ &\quad\times\cos\left(kR_n-\alpha_n-\angle K-\angle h_{n_\nu}\right)\\ &\quad\left.\times\sin\left(kR_n-\alpha_n-\angle K-\angle h_{n_\xi}\right)\right\}\end{aligned}\tag{14}$$

allows to compute $\mathscr{K}_{x_\Re x_\Im}(P)$, $\mathscr{K}_{x_\Re y_\Im}(P)$, $\mathscr{K}_{x_\Re z_\Im}(P)$, $\mathscr{K}_{y_\Re x_\Im}(P)$, $\mathscr{K}_{y_\Re y_\Im}(P)$, $\mathscr{K}_{z_\Re x_\Im}(P)$, $\mathscr{K}_{y_\Re z_\Im}(P)$, $\mathscr{K}_{z_\Re y_\Im}(P)$, and $\mathscr{K}_{z_\Re z_\Im}(P)$. Finally, the following covariance function $\mathscr{K}_{\nu_\Im\xi_\Im}(P)$ (for $\nu = x, y, z$ and $\xi = x, y, z$):

$$\begin{aligned}\mathscr{K}_{\nu_\Im\xi_\Im}(P) &= \overline{E_{\nu_\Im}E_{\xi_\Im}} - \overline{E_{\nu_\Im}}\,\overline{E_{\xi_\Im}}\\ &= |K|^2\sum_{n=1}^{N}\left\{\frac{p_n\left(A_n^2+\sigma_{\delta A_n}^2\right)}{R_n^2}\left|h_{n_\nu}\right|\left|h_{n_\xi}\right|\right.\\ &\quad\times\left[\frac{1}{2}\cos\left(\angle h_{n_\xi}-\angle h_{n_\nu}\right)\right.\\ &\quad\left.\left.-\frac{1}{2}e^{-2\sigma_{\delta\alpha_n}^2}\cos\left(2kR_n-2\alpha_n-2\angle K - \angle h_{n_\nu}-\angle h_{n_\xi}\right)\right]\right\}\end{aligned}$$

$$- |K|^2 \sum_{n=1}^{N} \left\{ \frac{p_n^2 A_n^2}{R_n^2} |h_{n_\nu}| |h_{n_\xi}| e^{-\sigma^2_{\delta\alpha_n}} \times \sin\left(kR_n - \alpha_n - \angle K - \angle h_{n_\nu}\right) \times \sin\left(kR_n - \alpha_n - \angle K - \angle h_{n_\xi}\right) \right\} \quad (15)$$

allows to compute $\sigma^2_{x_\mathfrak{z}}(P)$, $\sigma^2_{y_\mathfrak{z}}(P)$, $\sigma^2_{z_\mathfrak{z}}(P)$, $\mathscr{K}_{x_\mathfrak{z} y_\mathfrak{z}}(P)$, $\mathscr{K}_{x_\mathfrak{z} z_\mathfrak{z}}(P)$, and $\mathscr{K}_{y_\mathfrak{z} z_\mathfrak{z}}(P)$. As it can be seen, for the determination of the mean of the squared magnitude of the electric field, no assumption is made on the relationship existing between the components of the random vector $\underline{X}(P)$. Following a similar approach would be more tedious for determining the variance of $|\mathbf{E}|^2(P)$. Instead, it can be obtained quite easily if assuming that the components of $\underline{X}(P)$ are jointly Gaussian at the generic observation point P, i.e., $\underline{X}(P) \sim \mathscr{N}(\underline{\mu}(P), \underline{\underline{\mathscr{K}}}(P))$. This assumption can be justified by exploiting the multivariate form of the central limit theorem [40] when the number of antenna elements is large enough. Consequently, provided that this assumption is verified, the variance of the squared magnitude of the electric field can be written as follows [47]:

$$\sigma^2_{|\mathbf{E}|^2}(P) = 2\,tr\left\{\underline{\underline{\mathscr{K}}}(P) \cdot \underline{\underline{\mathscr{K}}}(P)\right\} + 4\,\underline{\mu}^T(P) \cdot \underline{\underline{\mathscr{K}}}(P) \cdot \underline{\mu}(P). \quad (16)$$

Although the mean and the variance of $|\mathbf{E}(P)|^2$ already provide some interesting information, they may also be exploited to obtain the following bounds for the cdf of $|\mathbf{E}(P)|^2$ by means of the Cantelli's inequality [38] (with τ being a real number):

$$\begin{cases} \mathscr{P}_r\left\{|\mathbf{E}(P)|^2 \le \overline{|\mathbf{E}(P)|^2} + \tau\right\} \le \dfrac{\sigma^2_{|\mathbf{E}|^2}(P)}{\sigma^2_{|\mathbf{E}|^2}(P) + \tau^2}, & \text{if } \tau < 0 \\ \mathscr{P}_r\left\{|\mathbf{E}(P)|^2 \le \overline{|\mathbf{E}(P)|^2} + \tau\right\} \ge 1 - \dfrac{\sigma^2_{|\mathbf{E}|^2}(P)}{\sigma^2_{|\mathbf{E}|^2}(P) + \tau^2}, & \text{if } \tau \ge 0 \end{cases} \quad (17)$$

where $\mathscr{P}_r\{\cdot\}$ is the probability measure. However, Cantelli's inequality provides only partial information on the effective distribution of the squared magnitude of the electric field. For this reason, a more in-depth characterization of $|\mathbf{E}(P)|^2$ is performed below to increase the information content.

A. Generalized Variance, Generalized Distance, and Possible Singularities of the Covariance Matrix

In this section, some crucial metrics related to the squared magnitude of the electric field are discussed. In particular, the discussion is relatively general here since the assumption of Gaussianity is not used for the components of $\underline{X}(P)$. In the following, some helpful concepts to support the results of the other sections are reported. The first useful quantity to consider is the *generalized variance*, which coincides with the determinant of the covariance matrix [47]

$$GV(P) = \left|\underline{\underline{\mathscr{K}}}(P)\right| = \prod_{i=1}^{6} \eta_i^2(P) \quad (18)$$

where $\{\eta_i^2(P)\}_{i=1}^6$ are the eigenvalues of $\underline{\underline{\mathscr{K}}}(P)$. To generalize beyond the 1-D case, as the values of $GV(P)$ increase, the dispersion of $\underline{X}(P)$ with respect to its mean $\underline{\mu}(P)$ also increases. Another important metric is the *standardized distance* of $\underline{X}(P)$ to $\underline{\mu}(P)$ [47]

$$SD(P) = \left[\underline{X}(P) - \underline{\mu}(P)\right]^T \cdot \underline{\underline{\mathscr{K}}}^{-1}(P) \cdot \left[\underline{X}(P) - \underline{\mu}(P)\right] = \underline{Z}^T(P) \cdot \underline{Z}(P) \quad (19)$$

where the components of the random vector $\underline{Z}(P)$ have zero means, unit variances, and they are also uncorrelated. The following deterministic version of $SD(P)$:

$$sd(P) = \left[\underline{x} - \underline{\mu}(P)\right]^T \cdot \underline{\underline{\mathscr{K}}}^{-1}(P) \cdot \left[\underline{x} - \underline{\mu}(P)\right] \quad (20)$$

represents the distance of a generic (deterministic) point $\underline{x}$ of the multivariate distribution of $\underline{X}(P)$ with respect to $\underline{\mu}(P)$, the latter representing the centroid of the multivariate distribution. The square root of $sd(P)$ is also called *Mahalanobis distance* [48]. If some components of $\underline{X}(P)$ can be "deterministically" derived from the other components, then the covariance matrix is singular, and the above definitions must be modified. In this case, the generalized variance can coincide with $|\underline{\underline{\mathscr{K}}}(P)|_+$ (*pseudo-determinant*), which is the product of all the positive eigenvalues of $\underline{\underline{\mathscr{K}}}(P)$. As regarding the generalized distance, it is obtained from (20) by considering $\underline{\underline{\mathscr{K}}}^+(P)$ (*Moore–Penrose inverse*) in place of $\underline{\underline{\mathscr{K}}}^{-1}(P)$.

Equation (18) plays a key role in the analysis methodology being discussed. In fact, as well known, the variance is an important dispersion metric for a random variable. For n-dimensional random variables (random vectors), although it is possible to define the variance for each individual component, it is also necessary to have a metric that provides information on the dispersion, in the n-dimensional space, that random vectors present with respect to their mean. For this purpose, the determinant of the covariance matrix is used as a generalization of the variance to the n-dimensional case. In particular, (18) is based on the spectral decomposition of symmetric matrices, through which it is possible to calculate the determinant of the latter as the product of their eigenvalues [48].

IV. Mean Squared Errors

On the basis of the results obtained in the previous section, it is possible to define some error functions aimed at characterizing the *distance* between the actual electric field and the ideal one, and between the actual squared magnitude of the electric field and the desired one. It is worth highlighting that the variance of $\mathbf{E}(P)$ characterizes the dispersion of the actual electric field with respect to its mean, this latter being different from the ideal electric field. For this reason, by considering the random error function $\boldsymbol{\epsilon}(P) = \mathbf{E}(P) - \mathbf{E}_{id}(P)$, the mean of the squared magnitude of this function can be assumed as first metric, which coincides with the mean squared error between the actual electric field and the ideal one, namely

$$MSE(P) = \overline{|\boldsymbol{\epsilon}(P)|^2} = \sigma^2(P) + |\mathbf{E}_{id}(P) - \boldsymbol{\mu}(P)|^2. \quad (21)$$

In the absence of errors, the variance of the electric field is equal to zero, the mean of the actual electric field coincides with $\mathbf{E}(P)$, and, consequently, the function $MSE(P)$ function equals zero. The function $MSE(P)$ can also be normalized with respect to $|\mathbf{E}_{id}(P)|^2$, to obtain a sort of relative mean squared error between $\mathbf{E}(P)$ and $\mathbf{E}_{id}(P)$. However, strictly speaking, this normalization is more suitable if the mean squared error between $|\mathbf{E}(P)|^2$ and $|\mathbf{E}_{id}(P)|^2$ is considered, namely

$$\begin{aligned} MSE_{|\mathbf{E}|^2}(P) &= \overline{\left\{|\mathbf{E}(P)|^2 - |\mathbf{E}_{id}(P)|^2\right\}^2} \\ &= \overline{|\mathbf{E}(P)|^4} + |\mathbf{E}_{id}(P)|^4 - 2\,\mu_{|\mathbf{E}|^2}(P)\,|\mathbf{E}_{id}(P)|^2 \\ &= \mu^2_{|\mathbf{E}|^2}(P) + \sigma^2_{|\mathbf{E}|^2}(P) + |\mathbf{E}_{id}(P)|^4 \\ &\quad - 2\mu_{|\mathbf{E}|^2}(P)\,|\mathbf{E}_{id}(P)|^2. \end{aligned} \tag{22}$$

In this case, the function $MSE_{|\mathbf{E}|^2}(P)/|\mathbf{E}_{id}(P)|^4$ coincides precisely with the *relative* mean squared error between $|\mathbf{E}(P)|^2$ and $|\mathbf{E}_{id}(P)|^2$.

V. Multivariate Characterization of the Squared Magnitude of the Electric Field and a Computation of Its Distribution

This section discusses the characterization of the squared magnitude of the electric field by exploiting the joint probability density function of the real and the imaginary parts of the components of the electric field. To this end, let us assume that the number of antenna elements is high enough to model, by exploiting a multivariate form of the central limit theorem [40], $\underline{X}(P)$ as a *multivariate Gaussian random vector*. Let us also assume, for the moment, that the covariance matrix is nonsingular. Consequently, at the generic point P, the joint probability density function of the components of $\underline{X}(P)$ can be written as follows (with $\underline{x} \in \mathbb{R}^6$):

$$f\left(\underline{x}; P\right) = \frac{1}{\sqrt{(2\pi)^N \left|\underline{\underline{\mathscr{K}}}(P)\right|}}\, e^{-\frac{1}{2}\left[\underline{x}-\underline{\mu}(P)\right]^T \cdot \underline{\underline{\mathscr{K}}}^{-1}(P)\cdot\left[\underline{x}-\underline{\mu}(P)\right]} \tag{23}$$

where $|\underline{\underline{\mathscr{K}}}(P)|$ is the determinant of the covariance matrix. The following expression (with $r \in \mathbb{R}$ constant):

$$\left[\underline{x} - \underline{\mu}(P)\right]^T \cdot \underline{\underline{\mathscr{K}}}^{-1}(P) \cdot \left[\underline{x} - \underline{\mu}(P)\right] = r^2 \tag{24}$$

represents the equation of a multidimensional ellipsoid, where the vector with variable components $\underline{x}$ belongs to the following locus of points [49]:

$$\underline{x} = \underline{\mu}(P) + r\,\underline{\underline{M}}(P) \cdot \underline{v} \tag{25}$$

and $\underline{v}$ is a vector with variable components such that $\underline{v}^T \cdot \underline{v} = 1$ and $\underline{\underline{\mathscr{K}}}(P) = \underline{\underline{M}}(P)\cdot\underline{\underline{M}}^T(P)$ is the Cholesky decomposition of the covariance matrix. Consequently, taking into account that, in this multivariate Gaussian case, the following random generalized distance:

$$\left[\underline{X}(P) - \underline{\mu}(P)\right]^T \cdot \underline{\underline{\mathscr{K}}}^{-1}(P) \cdot \left[\underline{X}(P) - \underline{\mu}(P)\right] = R^2(P) \tag{26}$$

is a χ^2 random variable with six degrees of freedom, it is relatively easy to determine the confidence regions for the random vector $\underline{X}(P)$. Indeed, it could be written that (with η being a real number)

$$\mathscr{P}_r\left\{R^2(P) \le \eta\right\} = \frac{\gamma(3, \eta/2)}{\Gamma(3)} \tag{27}$$

where $\gamma(s, t)$ is the *lower incomplete gamma function*, and $\Gamma(s)$ is the *gamma function* [50]. Consequently, it could be set $\mathscr{P}_r\{R^2(P) \le \eta_q(P)\} = q\%$ (with $0 \le q \le 100$ and $n = 6$), $\eta_q(P)$ being the qth percentile of $R^2(P)$, and then the qth n-dimensional ellipsoid, associated with $f(\underline{x}, P)$, can be determined by previously setting $r = \sqrt{\eta_q}$ and computing all the values of $\underline{x}$ satisfying (25). Once the vector with the highest Euclidean norm and satisfying (25) is identified, the approach in [37] can be generalized to the n-dimensional case. In fact, here, $q\%$ is the probability that $\underline{X}(P)$ lies inside the aforementioned ellipsoid. This is less than the probability that the same $\underline{X}(P)$ lies inside an n-dimensional sphere, centered at the origin, and having the above norm as radius. In case the covariance matrix is singular, the expressions (23)–(27) cannot be held valid. In fact, in (23) the pseudodeterminant $|\underline{\underline{\mathscr{K}}}(P)|_+$ and the Moore–Penrose pseudoinverse $\underline{\underline{\mathscr{K}}}^+(P)$ must be considered, instead of $|\underline{\underline{\mathscr{K}}}(P)|$ and $\underline{\underline{\mathscr{K}}}^{-1}(P)$, respectively [48]. Consequently, when the covariance matrix is singular, the treatment through the multidimensional pdf may become more complicated. However, it is worth noting that the previous discussion based on $f(\underline{x}, P)$ represents an important conceptual basis for the sequel, as it provides important information on the (spatial) distribution of the realizations of $\underline{X}(P)$ in the multidimensional space and, coherently to what stated above, it would lead to find a lower bound for the distribution of the squared magnitude of the actual electric field.

At this point, a more general methodology needs to be found which allows to *directly* overcome the problem of possible singularities of the covariance matrix, and to more easily find an estimate of the distribution of $|\mathbf{E}(P)|^2$. To this end, a particular representation of $\underline{X}(P)$ is exploited in the following to achieve the above goal. In this framework, the spectral decomposition of the covariance matrix can be written as follows [48]:

$$\underline{\underline{\mathscr{K}}}(P) = \sum_{i=1}^{6} \eta_i^2(P)\,\underline{u}_i(P) \cdot \underline{u}_i^T(P) \tag{28}$$

where $\{\eta_i^2(P)\}_{i=1}^6$ and $\{\underline{u}_i(P)\}_{i=1}^6$ are the eigenvalues and eigenvectors of $\underline{\underline{\mathscr{K}}}(P)$, respectively, with $\eta_1^2(P) \ge \eta_2^2(P) \ge \cdots \ge \eta_6^2(P) \ge 0$. The above eigenvectors form an orthonormal basis for $\mathbb{R}^6$, and thus the vector $\underline{X}(P) - \underline{\mu}(P)$ can be represented as follows [48]:

$$\underline{X}(P) - \underline{\mu}(P) = \sum_{i=1}^{6} w_i(P)\,\underline{u}_i(P) \tag{29}$$

where $\{w_i(P) = [\underline{X}(P) - \underline{\mu}(P)]^T \cdot \underline{u}_i(P)\}_{i=1}^6$ are independent Gaussian random variables. In particular, $w_i(P)$ is a Gaussian random variable with mean equal to zero and variance equal to $\eta_i^2(P)$. Therefore, the squared magnitude of the electric field can be written as follows:

$$|\mathbf{E}(P)|^2 = \underline{X}^T(P) \cdot \underline{X}(P)$$

$$= \sum_{i=1}^{6} w_i^2(P) + 2\sum_{i=1}^{6} \widetilde{\mu}_i(P)\, w_i(P) + \sum_{i=1}^{6} \widetilde{\mu}_i{}^2(P)$$
$$= \sum_{i=1}^{6} \eta_i^2(P)\left[\frac{w_i(P)}{\eta_i(P)}\right]^2 + 2\sum_{i=1}^{6} \widetilde{\mu}_i(P)\eta_i(P)\left[\frac{w_i(P)}{\eta_i(P)}\right]$$
$$+ \sum_{i=1}^{6} \widetilde{\mu}_i{}^2(P) \tag{30}$$

with $[w_i(P)/\eta_i(P)]^2$ and $[w_i(P)/\eta_i(P)]$ being a χ^2 random variable with one degree of freedom and a standard normal random variable (with mean equal to zero and unitary variance), respectively, while the generic $\widetilde{\mu}_i(P)$ is equal to $\underline{\mu}^T(P)\cdot\underline{u}_i(P)$. Consequently, the cdf of the squared magnitude of the electric field coincides with the cdf of a *generalized* χ^2 *random variable* [51]. It is worth emphasizing that, through the described (decomposition) approach, any singularities of the covariance matrix are naturally taken into consideration, since in this case, there are some coefficients w_i being identically zero, and therefore the summation in (30) is simply composed of a number of terms less than six.

To the best of the authors' knowledge, there is no closed-form for the distribution of a generalized χ^2 random variable. However, it is worth highlighting that the squared magnitude of the electric field is now described in terms of a linear combination of six independent χ^2 random variables with one degree of freedom, plus a linear combination of six independent normal random variables, plus a deterministic term. Consequently, since the number of terms in (30) is sufficiently low, the Monte Carlo method can be advantageously exploited to determine the distribution of $|\mathbf{E}(P)|^2$. It is also worth specifying that, in practice, the linear combination of the χ^2 random variables cannot be generated independently of the linear combination of normal random variables, i.e., to determine the realizations of $|\mathbf{E}(P)|^2$ using the Monte Carlo method, only numerous different sets $\{w_i(P)\}_{i=1}^6$ are generated and subsequently the relation (30) is implemented. More advantageously, it is sufficient to generate a large number of standard normal random variables once at all, in such a way to exploit them for all the generic observation points at which the distribution of the squared magnitude of the electric field must be determined. As it can be seen in the sequel, there is an excellent matching between the empirical and the theoretical distribution. Once the distribution of $|\mathbf{E}(P)|^2$ is estimated, the related qth percentile function, $e_q(P)$, can be determined as before, namely (with $0 \le q \le 100$)

$$\mathscr{P}_r\left\{|\mathbf{E}(P)|^2 \le e_q(P)\right\} = q\% \tag{31}$$

where $e_q(P)$ coincides precisely with the qth percentile of the random variable $|\mathbf{E}(P)|^2$.

Now, an important aspect is worth highlighting. The expressions (28)–(30) hold even when $\underline{X}(P)$ is not a multidimensional normal random vector. However, in the general case, although the coefficients $\{w_i\}_{i=1}^6$ are still uncorrelated with each other, since the eigenvectors of $\underline{\underline{\mathscr{K}}}(P)$ are an orthonormal system [48], it cannot be asserted that these coefficients are also independent nor that they are normal random variables. However, as shown in the following section, even when the number of radiators is relatively small, the present methodology proves to be effective.

VI. Numerical Results

In this section, suitable numerical results are discussed to show the validity of the proposed methodology. Elementary dipoles are assumed as radiators [42], taking into account that the antenna element does not strongly affect the intrinsic performance of the array [52]. Consequently, the expression for the actual total electric field can be written as follows:

$$\mathbf{E}(P) = K\,\Delta z \sum_{n=1}^{N}\Bigg\{F_n(A_n+\delta A_n)\,e^{j(\alpha_n+\delta\alpha_n)}\frac{e^{-jkR_n}}{R_n} \times\left[\frac{(x-x_n)(z-z_n)}{R_n^2}\hat{\mathbf{x}} + \frac{y(z-z_n)}{R_n^2}\hat{\mathbf{y}} - \frac{(x-x_n)^2+y^2}{R_n^2}\hat{\mathbf{z}}\right]\Bigg\} \tag{32}$$

where $\Delta z \ll \lambda$ is the dipole length, λ is the wavelength in the propagation medium, and, as before, the operator $\times$ denotes the scalar multiplication. In particular, the dipole length is set equal to $\Delta z = \lambda/50$, although the present methodology does not depend on its actual value. For each n, it results: $A_n = 1$ A, $\sigma_{\delta A_n} = 0.2$ A, $\sigma_{\delta\alpha_n} = 0.2$ rad, $m_n = 0.97$. As a first case, a $N = N_x \times N_z = 11 \times 11 = 121$ periodic planar array is considered in which both the spacings along x and z are equal to λ, with N_x and N_z being the number of antenna elements along the x- and z-axis, respectively, (see Fig. 1). Subsequently, the case where $N = N_x \times N_z = 6 \times 6 = 36$ is also considered, in order to show that the theoretical results can be exploited even when the total number of antenna elements is relatively low. For the examples below, the focal point is at $(x_f, y_f, z_f) = (0, 20\,\lambda, 0)$ for the first case ($N = 121$), while it is at $(x_f, y_f, z_f) = (0, 10\,\lambda, 0)$ for the second case ($N = 36$).

Fig. 2 shows the comparison between the normalized square magnitude of the ideal electric field [Fig. 2(a)], the normalized square magnitude of the mean of the actual electric field [Fig. 2(b)], the normalized mean squared magnitude of the electric field [Fig. 2(c)], and a realization of the squared magnitude of the actual electric field [Fig. 2(d)] in the plane of focus. As can be seen, the functions $|\mathbf{E}_{id}(P)|^2/\max\{|\mathbf{E}_{id}(P)|^2\}$ and $|\boldsymbol{\mu}(P)|^2/\max\{|\boldsymbol{\mu}(P)|^2\}$ exhibit almost the same behavior; instead, the normalized mean squared magnitude of the electric field presents a behavior similar to the first two functions in the cuts $x/\lambda = 0$ and $z/\lambda = 0$, while, as compared to these, it shows significantly higher secondary lobes (relative with respect to the maximum value). This is consistent with the tolerance theory of far-field arrays, where the mean square magnitude of the array factor has a dominant term proportional to the squared magnitude of the ideal array factor, plus an additive error term which leads to a rise in the secondary lobe levels. The average behavior of the actual squared magnitude of the electric field is obviously also reflected in the realizations (sample paths) of $|\mathbf{E}(P)|^2$. Actually, observing Fig. 2(d), it can be recognized that the errors induce not only an elevation of the relative

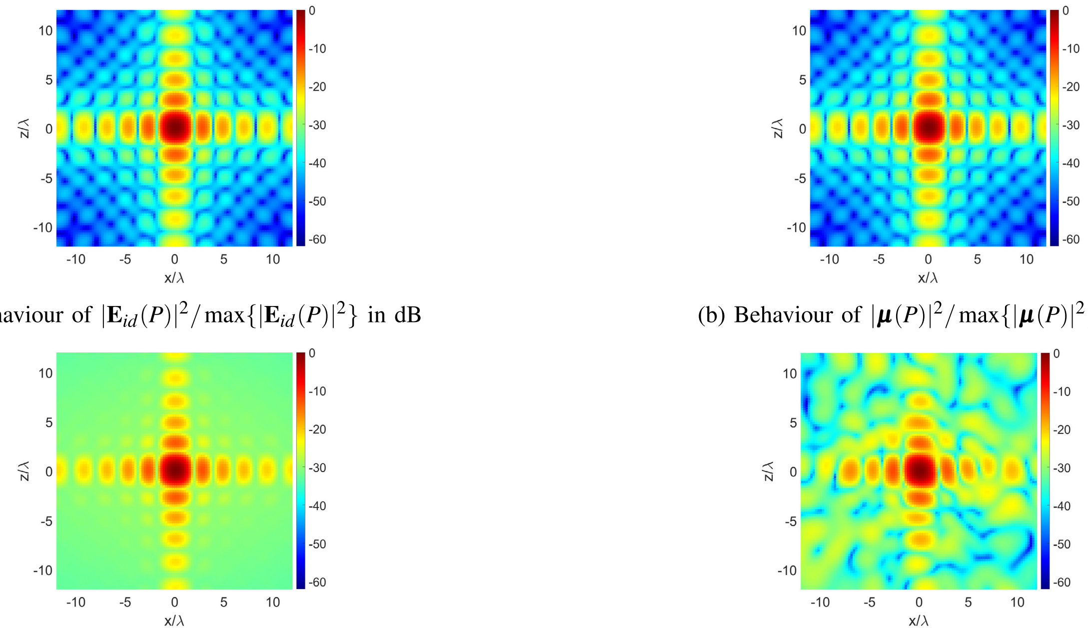

(a) Behaviour of $|\mathbf{E}_{id}(P)|^2/\max\{|\mathbf{E}_{id}(P)|^2\}$ in dB

(b) Behaviour of $|\boldsymbol{\mu}(P)|^2/\max\{|\boldsymbol{\mu}(P)|^2\}$ in dB

(c) Behaviour of $\mu_{|\mathbf{E}|^2}(P)/\max\{\mu_{|\mathbf{E}|^2}(P)\}$ in dB

(d) Behaviour of $|\mathbf{E}(P)|^2/\max\{|\mathbf{E}(P)|^2\}$ in dB

Fig. 2. Comparison, in the focal plane, between (a) normalized squared magnitude of the ideal electric field, (b) normalized squared magnitude of the mean of the actual electric field, (c) normalized mean of the squared magnitude of the actual electric field, and (d) normalized sample path of the squared magnitude of the actual electric field. The number of antenna elements is $N = N_x \times N_z = 11 \times 11$.

(a) Empirical standard deviation of $|\mathbf{E}(P)|^2$

(b) Theoretical standard deviation of $|\mathbf{E}(P)|^2$

Fig. 3. Comparison, in the focal plane, between (a) empirical and (b) theoretical standard deviation of the squared magnitude of the electric field. The number of antenna elements is $N = N_x \times N_z = 11 \times 11$ and the values are in linear scale.

levels of the secondary lobes, but also a distortion to the structure of the $|\mathbf{E}(P)|^2$. This confirms that it is important to consider the errors effect in near-field focused arrays, mainly if employed in high-performance scenarios. Fig. 3 compares the empirical standard deviation of the squared magnitude of the electric field, coinciding with the experimental variance of 2000 realizations of $|\mathbf{E}(P)|^2$, and the theoretical variance obtained by implementing (16). Observing the two figures, it can be noticed that (16) provides an excellent estimate of the variance of $|\mathbf{E}(P)|^2$.

Now, let us evaluate the validity of the methodology proposed in Section V. Fig. 4 compares, at the focal point, the empirical and the theoretical cdfs of the squared magnitude of the actual electric field. The empirical distribution is obtained through 2000 realizations of the random variable $|\mathbf{E}(P)|^2$ (ψ denoting the values assumed by $|\mathbf{E}(P)|^2$, i.e., $F(\psi) = \mathscr{P}_r\{|\mathbf{E}(P)|^2 \leq \psi\}$), the latter obtained from the squared magnitude of (3). Instead, the *theoretical* distribution is obtained by means of (28)–(30). Furthermore, the behaviors of the second

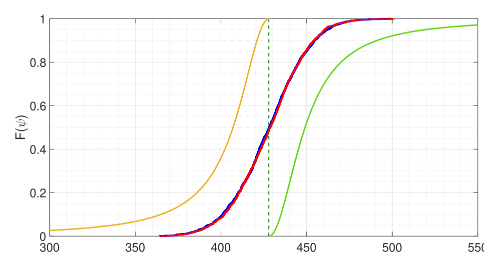

Fig. 4. Empirical (blue line) and theoretical (red line) cdf of the squared magnitude of the electric field at the focal point, together with the second members of the expressions related to Cantelli's inequality (orange line for $\tau < 0$, green line for $\tau \geq 0$). The number of antenna elements is $N = N_x \times N_z = 11 \times 11$. The values of ψ are in linear scale.

members of the expressions related to Cantelli's inequality are also shown. In particular, the orange line shows the behavior of $\sigma^2_{|\mathbf{E}|^2}(P)/[\sigma^2_{|\mathbf{E}|^2}(P) + \tau^2]$, the green curve is related to $1 - \{\sigma^2_{|\mathbf{E}|^2}(P)/[\sigma^2_{|\mathbf{E}|^2}(P) + \tau^2]\}$, and the vertical dotted purple line crosses the abscissa axis at the mean of $|\mathbf{E}(P)|^2$. As it

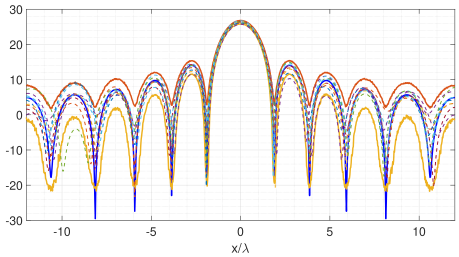

Fig. 5. Squared magnitude of the ideal electric field (blue solid line), 99th percentile function of the squared magnitude of the actual electric field (solid red line), first percentile function of the squared magnitude of the actual electric field (solid orange line), and various sample paths of the squared magnitude of the actual electric field (dashed lines) along the axis parallel to the x-axis and intersecting the y-axis at the focal point. The values on the abscissa axis are in linear scale, while those on the ordinate axis are in dB. The number of radiators is $N = N_x \times N_z = 11 \times 11$.

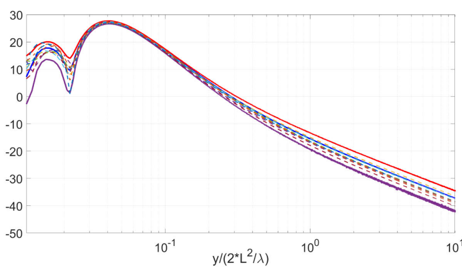

Fig. 6. Squared magnitude of the ideal electric field (blue solid line), 99th percentile function of the squared magnitude of the actual electric field (solid red line), first percentile function of the squared magnitude of the actual electric field (solid purple line), and various sample paths of the squared magnitude of the actual electric field (dashed lines) along the axis perpendicular to the array aperture and containing the focal point. The values on the abscissa axis are in logarithmic scale, while those on the ordinate axis are in dB. The number of radiators is $N = N_x \times N_z = 11 \times 11$.

can be seen, Cantelli's inequality provides bounds relatively far away from the actual distribution of $|\mathbf{E}(P)|^2$, if compared to the theoretical distribution obtained by the procedure described in Section V.

To further confirm the validity of the proposed methodology, in Fig. 5, it is illustrated the behavior of the field along the axis parallel to the x-axis and passing through the focal point, while in Fig. 6, the behavior of the field along y-axis, containing the focal point, is reported ($L = \sqrt{L_x^2 + L_z^2}$, with L_x and L_z being the lengths of the sides of the array). In particular, the above figures report the squared magnitude of the ideal electric field (blue solid line), the 99th percentile function (solid red line), the first percentile function (solid purple line), and different realizations of $|\mathbf{E}(P)|^2$ (dashed lines). By observing both figures, the percentile functions represent good estimates for the boundaries of the region encompassing most of the values of the squared magnitude of the electric field. In this way, it can provide important information on electric field levels for applications where high reliability is required. Of course, other percentile functions can be considered, depending on the safety margins needed.

Now, to test the impact that errors have on the performance of NFFAs when the number of radiators is relatively small and to verify whether the proposed methodology is valid even in this case, some results are shown for $N = N_x \times N_z = 6 \times 6$. Fig. 7 compares the functions $|\mathbf{E}_{id}(P)|^2/\max\{|\mathbf{E}_{id}(P)|^2\}$, $|\boldsymbol{\mu}(P)|^2/\max\{|\boldsymbol{\mu}(P)|^2\}$, $\mu_{|\mathbf{E}|^2}(P)/\max\{\mu_{|\mathbf{E}|^2}(P)\}$ and a realization of $|\mathbf{E}|^2(P)/\max\{|\mathbf{E}|^2(P)\}$. As before, the squared magnitude of the (ideal) electric field and the squared magnitude of the mean of the electric field have the same behavior in terms of focal spot shape and sidelobes structure; instead, the mean of the squared magnitude of the electric field has a higher relative sidelobe level, which is reflected in the realization of the squared magnitude of the electric field. Fig. 8 compares the empirical and the theoretical distributions of $|\mathbf{E}(P)|^2$, together with the function $\sigma^2_{|\mathbf{E}|^2}(P)/[\sigma^2_{|\mathbf{E}|^2}(P) + \tau^2]$, the green curve is related to $1 - \{\sigma^2_{|\mathbf{E}|^2}(P)/[\sigma^2_{|\mathbf{E}|^2}(P) + \tau^2]\}$ related to (17), at the focal point. As before, the vertical purple dashed line crosses the abscissa axis at the mean of the squared magnitude of the electric field. Also in this case, the theoretical estimate of the distribution of $|\mathbf{E}(P)|^2$ obtained through the procedure described in Section V is satisfactory, while the bounds given by Cantelli's inequality are far from the actual values. Finally, Figs. 9 and 10 compare the squared magnitude of the ideal electric field, the 99th percentile function, the first percentile function, and different realizations of $|\mathbf{E}(P)|^2$ (dashed lines), as in Figs. 5 and 6. Again, the considered percentile functions provide a good delimitation of the region containing most of the values of $|\mathbf{E}(P)|^2$.

The results shown in this section have been considered the most significant for the purpose of sufficient validation of the proposed statistical analysis methodology. However, a numerical study based on the approach performed in [53] could also be conducted for a more in-depth analysis of the impact that errors exert on the performance of near-field focused arrays.

Before moving to the next section, it is worth asking whether the assumptions of Section II about mutual couplings can be justified. As an example, let us consider results obtained from full-wave simulations of a planar array of half-wavelength cylindrical dipoles (i.e., with noninfinitesimal diameters comparable to the lengths). As before, the dipoles are placed in the xz plane, and they are oriented along the z-axis. The focus point coincides with the point $(x_f, y_f, z_f) = (0, 6.8854\,\lambda, 0)$, and the nominal excitation coefficients all have the same magnitude. Fig. 11 shows the (normalized) squared magnitude of the electric field generated by the array at the focusing plane. In particular, Fig. 11(a) shows the theoretical squared magnitude of the electric field (i.e., dipoles with infinitesimal diameters) in which neither errors nor mutual coupling effects are considered. Fig. 11(b) shows the same quantity, but in the presence of only random errors (also in this case dipoles have infinitesimal diameters). As it can be seen, the presence of errors produces a distortion in the field structure, also causing an increase of the field level in the region of the secondary lobes. Fig. 11(c) and (d) shows the squared magnitude of the electric field obtained from full-wave simulations of the array, in the absence of errors, with dipoles having diameters equal to $\lambda/50$ and $\lambda/10$, respectively. Dipoles of this type can be considered *broadband* as compared to standard thin dipoles [9]. As it can be seen, in this case, the field distortion due to mutual couplings shows a smaller entity as compared to that caused by random errors.

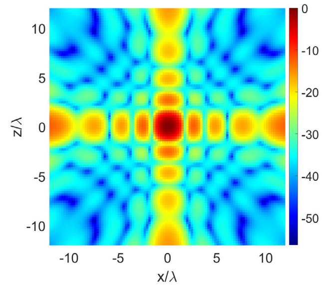

(a) Behaviour of $|\mathbf{E}_{id}(P)|^2/\max\{|\mathbf{E}_{id}(P)|^2\}$ in dB

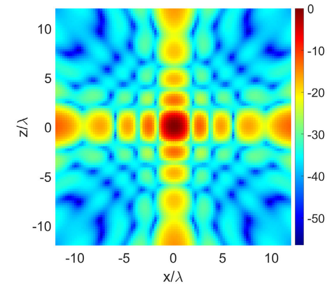

(b) Behaviour of $|\boldsymbol{\mu}(P)|^2/\max\{|\boldsymbol{\mu}(P)|^2\}$ in dB

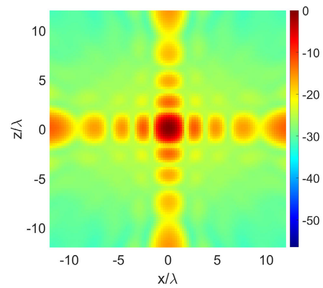

(c) Behaviour of $\mu_{|\mathbf{E}|^2}(P)/\max\{\mu_{|\mathbf{E}|^2}(P)\}$ in dB

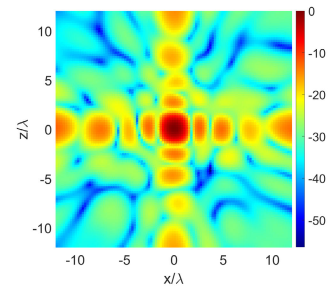

(d) Behaviour of $|\mathbf{E}(P)|^2/\max\{|\mathbf{E}(P)|^2\}$ in dB

Fig. 7. Comparison, in the focal plane, between (a) normalized squared magnitude of the ideal electric field, (b) normalized squared magnitude of the mean of the actual electric field, (c) normalized mean of the squared magnitude of the actual electric field, and (d) normalized sample path of the squared magnitude of the actual electric field. The number of antenna elements is $N = N_x \times N_z = 6 \times 6$.

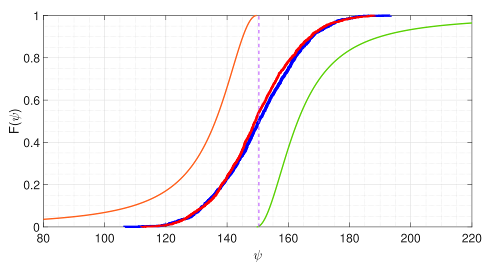

Fig. 8. Empirical (blue line) and theoretical (red line) cdf of the squared magnitude of the electric field at the focal point, together with the second members of the expressions related to Cantelli's inequality (orange line for $\tau < 0$, green line for $\tau \geq 0$). The number of antenna elements is $N = N_x \times N_z = 6 \times 6$. The values of ψ are in linear scale.

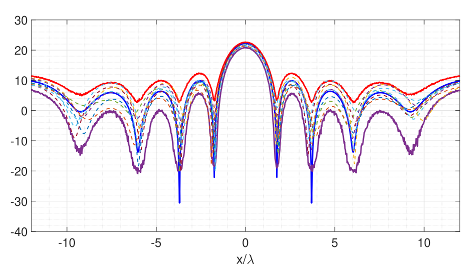

Fig. 9. Squared magnitude of the ideal electric field (blue solid line), 99th percentile function of the squared magnitude of the actual electric field (solid red line), first percentile function of the squared magnitude of the actual electric field (solid purple line), and various sample paths of the squared magnitude of the actual electric field (dashed lines) along the axis parallel to the x-axis and intersecting the y-axis at the focal point. The values on the abscissa axis are in linear scale, while those on the ordinate axis are in dB. The number of radiators is $N = N_x \times N_z = 6 \times 6$.

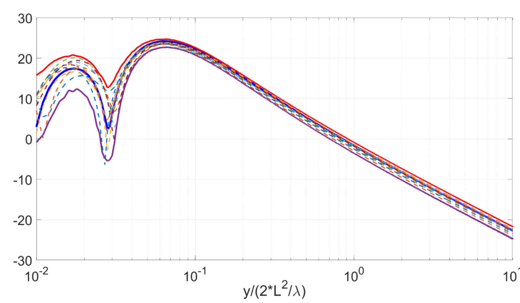

Fig. 10. Squared magnitude of the ideal electric field (blue solid line), 99th percentile function of the squared magnitude of the actual electric field (solid red line), first percentile function of the squared magnitude of the actual electric field (solid purple line), and various sample paths of the squared magnitude of the actual electric field (dashed lines) along the axis perpendicular to the array aperture and containing the focal point. The values on the abscissa axis are in logarithmic scale, while those on the ordinate axis are in dB. The number of radiators is $N = N_x \times N_z = 6 \times 6$.

Consequently, in such situations where errors predominate over mutual couplings (since the latter can be neglected or adequately compensated), the proposed methodology can be useful to have a more realistic characterization of near-field focused arrays.

VII. Experimental Results

In the present section, some experimental results are discussed to show the impact of errors on actual practical fields, as well as to highlight a possible link between the array tolerance theory and the array diagnostics [54]. Concerning this last aspect, in both cases, faults can be modeled through binary quantities multiplying the excitation coefficients. In principle, the array tolerance theory and the array diagnostics can be seen as different ways of dealing with the same problem, the first one being useful to obtain a priori information on the difference between the actual field and the nominal one, and the second one being useful to achieve a posteriori information

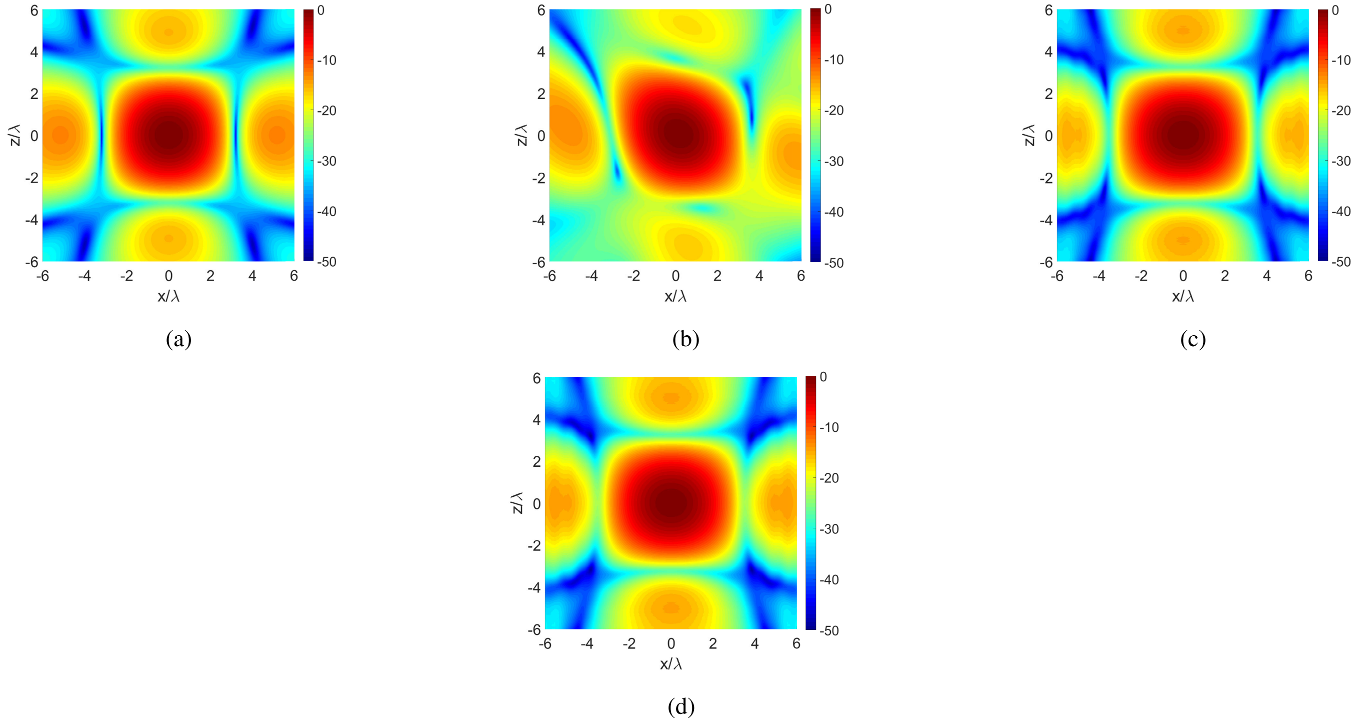

Fig. 11. Normalized squared magnitude of the electric field (in dB), at the focusing plane, for a planar array of 16 half-wavelength dipoles with uniform $0.6\,\lambda$ spacing in both directions. (a) Theoretical (ideal) case. (b) Theoretical case in the presence of random errors. (c) Full-wave simulation with dipoles diameter equal to $\lambda/50$. (d) Full-wave simulation with dipoles diameter equal to $\lambda/10$.

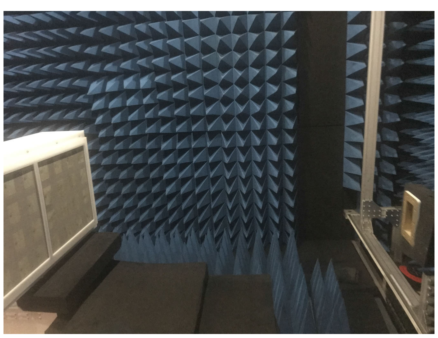

Fig. 12. Measurement setup into ERMIAS Laboratory at University of Calabria.

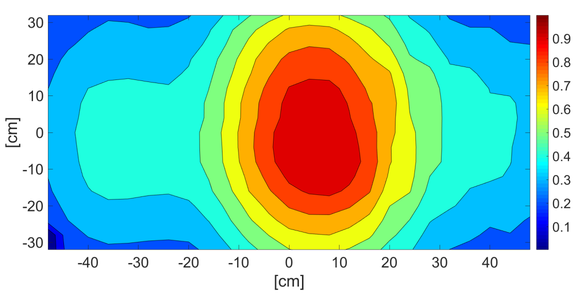

Fig. 13. Normalized amplitude of the measured near-field in the absence of errors (the values are in linear scale).

on the actual field with the aim to identify faulty array elements.

In Fig. 12, the measurement setup equipped into ERMIAS Laboratory at University of Calabria is illustrated. It includes a

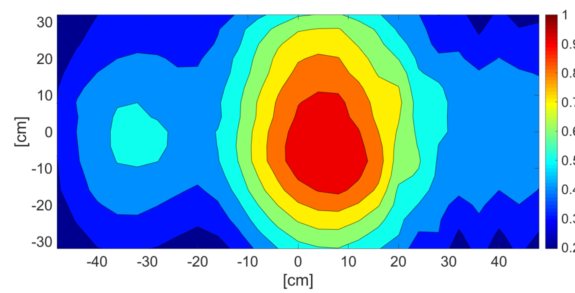

Fig. 14. Normalized amplitude of the measured near-field in the presence of errors (the values are in linear scale).

L-band planar array of microstrip rectangular patches, having an interelement spacing approximately equal to $0.6\,\lambda$, which is assumed as antenna under test (AUT). A standard rectangular waveguide working in the same frequency range is adopted as probe to perform the planar near-field measurements on a grid of 25×17 points along x and y directions, respectively, with a sampling step $\Delta x = \Delta y = \lambda/4$ at an operating frequency $f = 1.685$ GHz. In this experimental test case, the array is far-field focused in the direction perpendicular to the array aperture, but field measurements are performed in the Fresnel zone. It is worth highlighting that the characterization of random errors does not depend on whether the arrays are focused in the near zone or in the far zone. For comparison purposes, to highlight the field distortion effects of errors, in Figs. 13 and 14, the normalized squared magnitude of the measured electric field in the absence of errors and in the presence of element failures are reported, respectively.

VIII. Conclusion

A new methodology implementing a useful tolerance theory for near-field focused arrays has been proposed in this work, to characterize the statistical behavior of the full vector electric field in the presence of random errors affecting the performance of antenna arrays with arbitrary geometry. As a preliminary operation, a first- and second-order partial statistical characterization of the electric field has been performed. Subsequently, the mean squared errors between the actual and the desired electric field, and between the actual and the ideal squared magnitude of the electric field have been considered. Finally, the efficient computation of the cdf of the squared magnitude of the electric field is performed by considering the vector including both the real and the imaginary parts of the three complex scalar components modeled in terms of a multivariate Gaussian vector. Following the above procedure, suitable confidence regions for the electric field magnitude have been identified through proper percentile functions. In the present work, mutual couplings have been assumed to be weak enough so to avoid any influence on the vector structure of the electric or magnetic current densities. However, as a future goal, a procedure will be developed to consider the actual effective lengths, thus leading to include also the mutual coupling effects, so obtaining a more accurate analysis of the random errors impact on NFFAs. The proposed approach can be usefully adopted to guarantee human safety in all those microwave and RF applications adopting NFFAs.

Acknowledgment

The authors would like to thank Antonio Borgia for the precious support during the experimental stage.

References

[1] R. Hansen, "Focal region characteristics of focused array antennas," *IEEE Trans. Antennas Propag.*, vol. AP-33, no. 12, pp. 1328–1337, Dec. 1985.

[2] D. A. Hill, "A numerical method for near-field array synthesis," *IEEE Trans. Electromagn. Compat.*, vol. EMC-27, no. 4, pp. 201–211, Nov. 1985.

[3] M. Narasimhan, K. Varadarangan, and S. Christopher, "A new technique of synthesis of the near- or far-field patterns of arrays," *IEEE Trans. Antennas Propag.*, vol. AP-34, no. 6, pp. 773–778, Jun. 1986.

[4] M. S. Narasimhan and B. Philips, "Synthesis of near-field patterns of arrays," *IEEE Trans. Ant. Propag.*, vol. AP-35, no. 2, pp. 212–218, Feb. 1987.

[5] A. J. Fenn, C. J. Diederich, and P. R. Stauffer, "An adaptive-focusing algorithm for a microwave planar phased-array hyperthermia system," *Lincoln Lab. J.*, vol. 6, no. 2, pp. 269–288, 1993.

[6] T. C. Guo, W. W. Guo, and L. E. Larsen, "A local field study of a water-immersed microwave antenna array for medical imagery and therapy," *IEEE Trans. Microw. Theory Techn.*, vol. AP-32, no. 8, pp. 844–854, Aug. 1984.

[7] P. Nepa and A. Buffi, "Near-field-focused microwave antennas: Near-field shaping and implementation," *IEEE Antennas Propag. Mag.*, vol. 59, no. 3, pp. 42–53, Jun. 2017.

[8] Z. Chen, H. Sun, and W. Geyi, "Maximum wireless power transfer to the implantable device in the radiative near field," *IEEE Antennas Wireless Propag. Lett.*, vol. 16, pp. 1780–1783, 2017.

[9] R. L. Haupt, *Antenna Arrays: A Computational Approach*. Hoboken, NJ, USA: Wiley, 2010.

[10] R. E. Collin, "Radiation from apertures," in *Antenna Theory*, R. E. Collin and F. J. Zucker, Eds. New York, NY, USA: McGraw-Hill, 1969, ch. 3, sec. 3.7, pp. 86–89.

[11] B. D. Steinberg, *Principles of Aperture & Array System Design*. New York, NY, USA: Wiley, 1976.

[12] R. J. Mailloux, *Phased Array Antenna Handbook* (Artech House Antennas and Propagation Library), 2nd ed. 2005.

[13] J. Ruze, "Physical limitations on antennas," M.S. thesis, Dept. Elect. Eng., Massachusetts Inst. Technol., May 1952.

[14] J. Ruze, "Physical limitations on antennas," Res. Lab. Electron., Tech. Rep., 248, Oct. 1952.

[15] D. Ashmead, "Optimum design of linear arrays in the presence of random errors," *Trans. IRE Prof. Group Antennas Propag.*, vol. 4, no. 1, pp. 81–92, Dec. 1952.

[16] E. N. Gilbert and S. P. Morgan, "Optimum design of directive antenna arrays subject to random variations," *Bell Syst. Tech. J.*, vol. 34, no. 3, pp. 637–663, May 1955.

[17] L. A. Rondinelli, "Effects of random errors on the performance of antenna arrays of many elements," in *Proc. IRE Int. Conv. Rec.*, 1959, pp. 174–189.

[18] R. Elliott, "Mechanical and electrical tolerances for two-dimensional scanning antenna arrays," *IRE Trans. Antennas Propag.*, vol. 6, no. 1, pp. 114–120, Jan. 1958.

[19] J. L. Allen, "Some extension of the theory of random error effects on array patterns," Chapter III, Part 3 Phased Array Radar Stud., Lincoln Lab., Tech. Rep., 236, Nov. 1961.

[20] J. K. Hsiao, "Array sidelobes, error tolerances, gain and beamwidth," Naval Res. Lab., Washington, DC, USA, Tech. Rep., 1984.

[21] J. K. Hsiao, "Design of error tolerance of a phased array," *Electron. Lett.*, vol. 21, no. 19, pp. 834–836, 1985.

[22] R. D. Kaplan, "Predicting antenna sidelobe performance," *Microw. J.*, vol. 29, no. 9, pp. 201–204, 1986.

[23] M. I. Skolnik, "Nonuniform arrays," in *Antenna Theory*, R. E. Collin and F. Zucker, Eds. New York, NY, USA: McGraw-Hill, 1969.

[24] A. K. Bhattacharyya, *Phased Array Antennas: Floquet Analysis, Synthesis, BFNs and Active Array Systems*, 1st ed. Hoboken, NJ, USA: Wiley, 2006.

[25] Y. S. Shifrin, "Pioneer award: Statistical antenna theory: Formation and extension," *IEEE Aerosp. Electron. Syst. Mag.*, vol. 31, no. 8, pp. 24–36, Aug. 2016.

[26] A. J. van den Biggelaar, U. Johannsen, P. Mattheijssen, and A. B. Smolders, "Improved statistical model on the effect of random errors in the phase and amplitude of element excitations on the array radiation pattern," *IEEE Trans. Antennas Propag.*, vol. 66, no. 5, pp. 2309–2317, May 2018.

[27] Y.-W. Hsu, "Statistical model for approximating gains of arrays with unequal normally distributed errors," *IEEE Trans. Antennas Propag.*, vol. 70, no. 12, pp. 11653–11664, Dec. 2022.

[28] Y. Zhang, D. Zhao, Q. Wang, Z. Long, and X. Shen, "Tolerance analysis of antenna array pattern and array synthesis in the presence of excitation errors," *Int. J. Antennas Propag.*, vol. 2017, pp. 1–6, Jan. 2017.

[29] Y. Lo, "A mathematical theory of antenna arrays with randomly spaced elements," *IEEE Trans. Antennas Propag.*, vol. AP-12, no. 3, pp. 257–268, May 1964.

[30] Y. T. Lo, "Random periodic arrays," *Radio Sci.*, vol. 3, no. 5, pp. 425–436, May 1968.

[31] G. Buonanno and R. Solimene, "Generalised random binned antenna arrays," *Prog. Electromagn. Res. C*, vol. 78, pp. 129–143, 2017.

[32] G. Buonanno and R. Solimene, "Unequally-excited linear totally random antenna arrays for multi-beam patterns," *IET Microw., Antennas Propag.*, vol. 12, no. 10, pp. 1671–1678, Aug. 2018.

[33] K. Buchanan and G. H. Huff, "A stochastic mathematical framework for the analysis of spherically-bound random arrays," *IEEE Trans. Antennas Propag.*, vol. 62, no. 6, pp. 3002–3011, Jun. 2014.

[34] G. Buonanno and R. Solimene, "Unequally excited generalised random binned antenna arrays," *IET Microw., Antennas Propag.*, vol. 13, no. 14, pp. 2531–2538, Nov. 2019.

[35] G. Buonanno and R. Solimene, "Global characterization of linear statistically thinned antenna arrays," *IEEE Access*, vol. 9, pp. 119629–119640, 2021.

[36] H. Ochiai, P. Mitran, H. V. Poor, and V. Tarokh, "Collaborative beamforming for distributed wireless ad hoc sensor networks," *IEEE Trans. Signal Process.*, vol. 53, no. 11, pp. 4110–4124, Nov. 2005.

[37] G. Buonanno and S. Costanzo, "Fresnel-zone focused antenna arrays: Tolerance analysis for biomedical applications," *IEEE Trans. Antennas Propag.*, vol. 71, no. 9, pp. 7261–7272, Sep. 2023, doi: 10.1109/TAP.2023.3295493.

[38] G. Buonanno, S. Costanzo, and R. Solimene, "Broadband statistically designed thinned-binned array antennas," *IEEE Trans. Antennas Propag.*, vol. 71, no. 3, pp. 2454–2466, Mar. 2023.

[39] S. Costanzo and G. Buonanno, "Tolerance analysis of near-field arrays for biomedical applications," in *Proc. Photon. Electromagn. Res. Symp. (PIERS)*, Prague, Czech Republic, Jul. 2023, pp. 1997–2002, doi: 10.1109/piers59004.2023.10221459.

[40] W. Feller, *An Introduction to Probability Theory and Its Applications*, vol. 2. New York, NY, USA: Wiley, 1966.

[41] *IEEE Standard for Safety Levels With Respect to Human Exposure to Electric, Magnetic, and Electromagnetic Fields, 0 Hz to 300 GHz-Corrigenda 2*. IEEE Standard C95.1-2019/Cor2, 2020, pp. 1–15, doi: 10.1109/IEEESTD.2020.9238523.

[42] G. Franceschetti, *Electromagnetics: Theory, Techniques, and Engineering Paradigms*. Berlin, Germany: Springer, Jan. 1998.

[43] M. R. Pino, R. G. Ayestarán, P. Nepa, and G. Manara, "An overview on synthesis techniques for near-field focused antennas," in *Recent Wireless Power Transfer Technologies*. IntechOpen, Mar. 2020, doi: 10.5772/intechopen.89600.

[44] W. L. Stutzman and G. A. Thiele, *Antenna Theory and Design*, 3rd ed. New York, NY, USA: Wiley, 2013, pp. 308–311.

[45] T. A. Milligan, *Modern Antenna Design*, 1st ed. New York, NY, USA: McGraw-Hill, sec. 3.11, 2005.

[46] F. Caminita et al., "Reduction of patch antenna coupling by using a compact EBG formed by shorted strips with interlocked branch-stubs," *IEEE Antennas Wireless Propag. Lett.*, vol. 8, pp. 811–814, 2009.

[47] A. C. Rencher and G. B. Schaalje, *Linear Models in Statistics*, 2nd ed. Hoboken, NJ, USA: Wiley, 2008.

[48] K. Kanatani, *Statistical Optimization for Geometric Computation: Theory and Practice*. New York, NY, USA: Dover, Jul. 2005.

[49] M. Bensimhoun, "N-dimensional cumulative function, and other useful facts about Gaussians and normal densities," Tech. Rep., 2009.

[50] M. Zelen and N. C. Severo, "Probability functions," in *Handbook of Mathematical Functions With Formulas, Graphs and Mathematical Tables* (National Bureau of Standards Applied Mathematics Series), M. Abramowitz and I. A. Stegun, Eds. Dec. 1972.

[51] A. Das and W. S. Geisler, "A method to integrate and classify normal distributions," *J. Vis.*, vol. 21, no. 10, Sep. 2021, doi: 10.1167/jov.21.10.1.

[52] A. Buffi, P. Nepa, and G. Manara, "Design criteria for near-field-focused planar arrays," *IEEE Antennas Propag. Mag.*, vol. 54, no. 1, pp. 40–50, Feb. 2012.

[53] G. Buonanno and R. Solimene, "Comparing different schemes for random arrays," *Prog. Electromagn. Res. B*, vol. 71, pp. 107–118, 2016.

[54] R. Palmeri, T. Isernia, and A. F. Morabito, "Diagnosis of planar arrays through phaseless measurements and sparsity promotion," *IEEE Antennas Wireless Propag. Lett.*, vol. 18, no. 6, pp. 1273–1277, Jun. 2019.

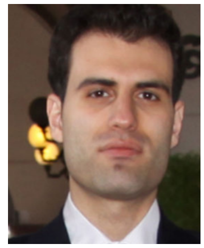

Giovanni Buonanno (Member, IEEE) received the M.S. degree (summa cum laude) in electronic engineering from the Seconda Università degli Studi di Napoli (SUN), Aversa, Italy, in 2014, and the Ph.D. degree in industrial and information engineering from the University of Campania, Caserta, Italy, in 2018.

After his M.S. he joined the Research Group in Applied Electromagnetics, SUN. He defended his Ph.D. thesis, in January 2019. He is currently with the University of Calabria, Rende, Italy. His research interests include nonuniformly spaced random arrays, biomedical signal processing, machine learning in electromagnetics, and tolerance analysis of antenna arrays.

Sandra Costanzo (Senior Member, IEEE) received the Laurea degree (summa cum laude) in computer engineering from Università della Calabria, Rende, Italy, in 1996, and the Ph.D. degree in electronic engineering from the Università Mediterranea di Reggio Calabria, Reggio Calabria, Italy, in 2000.

She is currently a Full Professor of electromagnetic fields with the Università della Calabria, where she is a Rector's Delegate for Health Safety. She teaches courses on electromagnetic waves propagation, antennas, remote sensing, radar, sensors, and electromagnetic diagnostics. She has authored or coauthored more than 230 contributions in international journals, books, and conferences. Her research interests are focused on near-field/far-field techniques, antenna measurement techniques, antenna analysis and synthesis, numerical methods in electromagnetics, millimeter wave antennas, reflectarrays, synthesis methods for microwave structures, electromagnetic characterization of materials, biomedical applications, and radar technologies.

Dr. Costanzo is the Vice-Chair of the IEEE MTT-28 Biological Effects and Medical Applications Committee, a member of the IEEE South Italy Geoscience and Remote Sensing Chapter, the Consorzio Nazionale Interuniversitario per le Telecomunicazioni (CNIT), the Società Italiana di Elettromagnetismo (SIEM), and the Centro Interuniversitario sulle Interazioni fra Campi Elettromagnetici e Biosistemi (ICEMB), and a Board Member of the IEEE AP/ED/MTT North Italy Chapter. She received the Telecom Prize for the Best Laurea Thesis in 1996, and the Best Academia and Research Application in Aerospace and Defense 2013 Award for the Application Software Defined Radar Using the NI USRP 2920 Platform. She is an Associate Editor Emeritus of IEEE JOURNAL OF ELECTROMAGNETICS, RF AND MICROWAVES IN MEDICINE AND BIOLOGY, an Associate Editor of IEEE ACCESS, a Section Editor of *Sensors* (section *Physical Sensors*), *Electronics* (section *Microwave and Wireless Communications*), *Polymers* (section *Smart and Functional Polymers Section*), an Editorial Board Member of *Radioengineering* and *International Journal of RF and Microwave Computer-Aided Engineering*. She is an Editor of the books titled *Microwave Materials Characterization* (INTECH, 2012) and *Wave Propagation Concepts for Near-Future Telecommunication Systems* (INTECH, 2017). She is a Lead Editor of more than 12 Special Issues on international journals.

Open Access funding provided by 'Università della Calabria' within the CRUI CARE Agreement